Cell Reports
Physical Science

CellPress
OPEN ACCESS

Article

Color-tunable hybrid heterojunctions as semi-transparent photovoltaic windows for photoelectrochemical water splitting

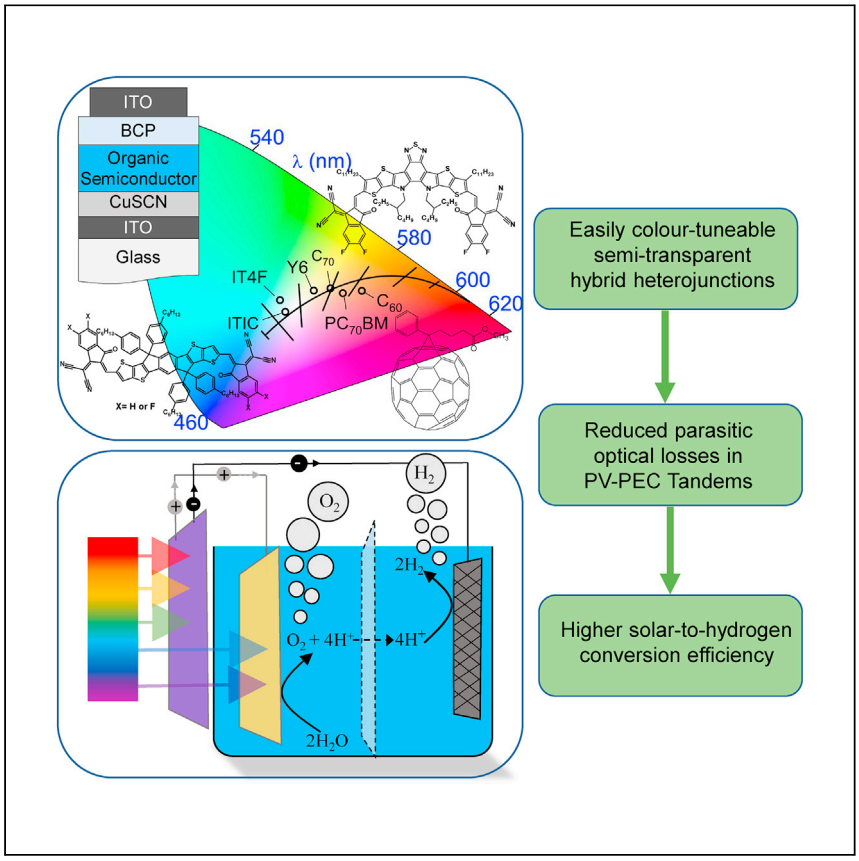

By combining the transparent inorganic semiconductor CuSCN with organic semiconductors, Eisner et al. model simple and inexpensive color-tunable semi-transparent photovoltaic windows. They further demonstrate that such photovoltaic windows can be used in conjunction with photoelectrochemical cells to reduce parasitic optical losses and increase the efficiency of sustainable solar hydrogen production.

Flurin Eisner, Brian Tam, Valentina Belova, ..., Mariano Campoy-Quiles, Anna Hankin, Jenny Nelson

f.eisner15@imperial.ac.uk (F.E.)
jenny.nelson@imperial.ac.uk (J.N.)

Highlights

Hybrid heterojunctions are color tunable through choice of organic semiconductor

Color-tunable semi-transparent photovoltaic windows with high photovoltage

Reduced parasitic optical absorption with photovoltaic windows in PV-PEC tandems

Higher solar-to-hydrogen efficiency compared with traditional configuration

Eisner et al., Cell Reports Physical Science 2, 100676
December 22, 2021
https://doi.org/10.1016/j.xcrp.2021.100676

Cell Reports
Physical Science

CellPress
OPEN ACCESS

Article

Color-tunable hybrid heterojunctions as semi-transparent photovoltaic windows for photoelectrochemical water splitting

Flurin Eisner,[1,5,*] Brian Tam,[1,2] Valentina Belova,[3] Wesley Ow,[1] Jun Yan,[1] Mohammed Azzouzi,[1] Andreas Kafizas,[2] Mariano Campoy-Quiles,[3] Anna Hankin,[4] and Jenny Nelson[1,*]

SUMMARY

The strong but narrow-bandwidth absorption spectra of organic semiconductors make them excellent candidates for semi-transparent solar cell applications in which color specificity is important. In this study, using a hybrid heterojunction combining the transparent inorganic semiconductor copper thiocyanate (CuSCN) with organic semiconductors (C_{70}, $PC_{70}BM$, C_{60}, ITIC, IT-4F, or Y6), we show that simple color-tunable solar cells can be fabricated in which the transmission spectrum is determined solely by choice of the organic semiconductor. Using a joint electrical-optical model, we show that it is possible to combine the unique attributes of high photovoltage and color tunability to use these heterojunctions as photovoltaic windows in tandem photoelectrochemical (PEC)-photovoltaic (PV) cells. We demonstrate that this configuration can lead to a reduction in the parasitic absorption losses in the PEC-PV cells and, thus, to solar-to-hydrogen efficiencies (>3%) that are higher than that predicted using the traditionally used architecture in which the PV is placed behind the PEC.

INTRODUCTION

Organic semiconductors tend to have narrow absorption bands, often in conjunction with high maximum absorption coefficients (>10^5 cm^{-1}) in the absorption region. This characteristic is a mixed blessing; the narrow absorption bands result in absorption of only a fraction of the available photons but allows specific tuning of the absorption range optimized to each device application; for example, in semitransparent solar cells. Additionally, the high absorption coefficient allows organic absorption layers to be orders of magnitude thinner than layers of inorganic semiconductors, such as silicon, without sacrificing photon absorption at the relevant wavelengths.

This unique property of organic semiconductors has been widely exploited in a number of opto-electronic applications, most notably in narrow-bandwidth organic photodetectors and semitransparent photovoltaic cells. Indeed, semi-transparent (ST) photovoltaic (PV) cells are recognized as one of the most promising short-term market niches of organic photovoltaics,[1–3] with potential applications in self-powered greenhouses,[4–6] power-generating heat insulation,[7] and windows.[8,9] Further, the color tunability of organic semiconductors is also useful for fabricating tandem devices where the color spectrum is shared, such as tandem PV-PV or photoelectrochemical-PV cells, allowing facile matching of photocurrents in each component while minimizing absorption losses.

[1]Department of Physics, Imperial College London, South Kensington, London SW7 2AZ, UK

[2]Department of Chemistry, Molecular Sciences Research Hub, Imperial College London, White City, London W12 0BZ, UK

[3]Nanostructured Materials Department, Material Science Institute of Barcelona, ICMAB-CSIC, 08193 Bellaterra, Spain

[4]Department of Chemical Engineering, Imperial College London, South Kensington, London SW7 2AZ, UK

[5]Lead contact

*Correspondence: f.eisner15@imperial.ac.uk (F.E.), jenny.nelson@imperial.ac.uk (J.N.)

https://doi.org/10.1016/j.xcrp.2021.100676

Although impressive advances have been made recently in color-tunable and organic semiconductor ST PV cells, a complication is the requirement for organic PVs to combine two organic semiconductors, a donor and an acceptor, to efficiently separate charges. This requirement means that the color spectrum of the photoactive component of any device depends on the combined optical profile of the (generally) mixed phase of the two materials. In-depth knowledge of the optical profile of the pristine materials and the phase behavior of the mixed materials is therefore required to accurately predict the device color spectrum using optical simulations.[10,11] Although tuneability could be improved by using a donor and acceptor of similar spectral response and band gap, the requirement for an offset in ionization potential and electron affinity of the components to maintain efficient charge generation limits the open-circuit voltage of such a device. For this reason, to obtain a high open circuit voltage (V_{oc}) in ST solar cells, a narrow-band-gap, non-fullerene acceptor is often paired with a medium-band-gap polymer donor with a high lowest unoccupied molecular orbital (LUMO), which constrains the transmissibility of the device.[12] For example, when substituting the wide-band-gap polymer PM6 in the state-of-the-art bulk heterojunction blend PM6:Y6-BO with a low-band-gap polymer of a band gap comparable with Y6-BO to achieve greater low-wavelength transparency, a reduction in the V_{oc} of 0.1 V is obtained in the resulting solar cell.[13]

An alternative to organic optoelectronic devices is a device comprising a solution-processed hybrid organic-inorganic heterojunction. This architecture opens the potentially advantageous possibility of pairing easily color-tunable organic semiconductors that display high absorption coefficients with highly crystalline and high-dielectric-constant inorganic semiconductors that aid charge generation across the hybrid.[14,15] We have demonstrated that planar hybrid heterojunctions consisting of the low-cost, p-type inorganic semiconductor copper thiocyanate (CuSCN) and various organic small-molecule acceptors allow efficient charge separation and, crucially, low non-radiative (0.21 V) V_{oc} losses.[16–20] Further, CuSCN is transparent to visible light, which means that the absorption profile of CuSCN/organic heterojunction devices is dominated completely by the organic semiconductor and, thus, offers the intriguing possibility of facile color-tunable optoelectronic devices.

Here, we use optical measurements and simulations to demonstrate that CuSCN/organic heterojunctions indeed offer the possibility of fabricating ST solar cells in which the absorption and transmission spectra are completely dominated by the choice of organic material. We show, using a theoretical model, that this allows facile fabrication of highly transmissive ST PV windows that can be easily tuned to suit specific applications (e.g., self-powered greenhouses, ST PV windows, and tandem cells). For one such application, photoelectrochemical-PV water-splitting tandem cells, we use an electro-optical model to show that such ST PV windows can be used successfully to minimize parasitic absorption losses through the tandem water-splitting device, which is a necessary condition to achieve high solar-to-hydrogen conversion efficiencies.

RESULTS

Color tunability and ST devices

In this study, we use the inorganic semiconductor CuSCN in a heterojunction with a range of the most successful organic solar cell acceptors: C_{70}, $PC_{70}BM$, C_{60}, ITIC, IT-4F, and Y6. Opaque devices fabricated with the simple and low-cost architecture indium tin oxide (ITO)/CuSCN/organic semiconductor/bathocuproine (BCP)/Al yield devices with power conversion efficiencies below 3% (Figures 1A and 1B; Tables S1

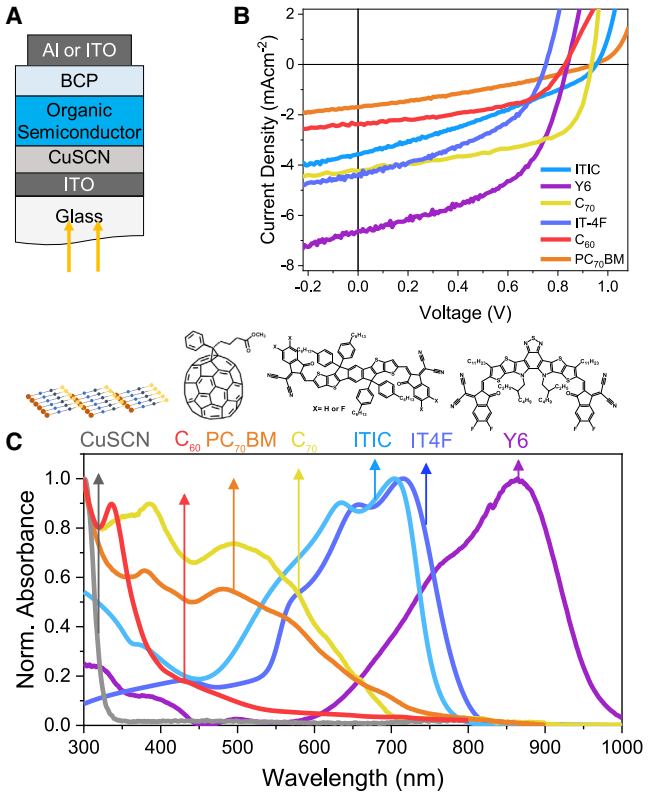

Figure 1. Device performance and thin film absorption spectra

(A) Device structure used in optical modeling of the devices, using an ITO top contact for ST devices and an Al contact for opaque devices. The direction of illumination (from the glass side) is shown.

(B) JV curves under AM1.5 illumination of opaque solar cells fabricated with different organic semiconductors on top of CuSCN.

(C) Normalized thin film absorption spectra measured by UV-vis (UV-vis) absorption of the materials used in the study. Shown also from left to right are the structures of CuSCN, $PC_{70}BM$, ITIC (without the fluorine atoms in red) and IT-4F (with the red fluorine atoms), and Y6.

Data for (B) and (C) are taken from Eisner et al.[20]

and S2) because of the limitation afforded by the exciton diffusion lengths of the organic semiconductor but with high internal quantum efficiencies of more than 70%.[20] Importantly, however, some of the devices, such as CuSCN/Y6, exhibit extremely low non-radiative voltage losses (down to 0.21 V) and are therefore suitable for applications with low-power, high-voltage needs. We predict that, by developing an intermixed CuSCN:organic semiconductor active layer, as we demonstrated previously with CuSCN:$PC_{70}BM$,[17] higher efficiencies would be within reach.

The normalized absorption spectrum of a CuSCN film is shown in Figure 1C and confirms previous results showing that CuSCN films are transparent to wavelengths longer than 320 nm.[21] The visible-light absorption spectrum of a device comprising a CuSCN/organic heterojunction is therefore dominated completely by the choice of organic material, a property that is especially attractive given the large number of recently developed n-type small molecules (non-fullerene acceptors [NFAs]) for use in organic bulk heterojunction devices, which display a range of absorption spectra. The normalized absorption spectra of the organic semiconductors used in the study are also shown in Figure 1C, displaying a range of absorption peaks from blue (fullerenes: C_{70} and $PC_{70}BM$), to red (ITIC and IT-4F), to near-infrared (Y6). The external quantum efficiency (EQE) responses of the devices are shown in Figure S1.

We exploit the color tunability of the materials by modeling the optical behavior of ST devices, which may be used, for example, as ST solar cell windows for greenhouses or for photoelectrochemical cells (PECs). To demonstrate such applications, we began by modeling the transmission, absorption, and reflection of ST devices using the same device architecture and active layer thickness we reported previously (ITO/CuSCN/organic/BCP/Al)[17,22] but replaced the top aluminum electrode with ITO and added an encapsulating layer of glass on top that would act as an impermeable layer to oxygen and water and enhance device lifetime. The optical constants of the materials were measured using ellipsometry (Figure S2), and a transfer matrix approach was used to model light propagation through the devices. Using alternative transparent electrode materials, such as silver nanowires or PEDOT:PSS would not significantly affect the optical modeling results. The resulting device transmission plots for optimized solar cell active-layer thickness are plotted in Figure 2A and show relatively narrow absorption peaks for each device, with high transparency at other wavelengths. As expected, simulated ST devices, calculated using the calculated internal quantum efficiency and assuming the superposition principle, showed a slight drop in performance compared with the measured opaque devices because of reduced reflection from the back cathode (Figure S3). From the device transmission spectra, we then calculate the transmission chromaticity of each device when illuminated with an AM1.5 spectrum, corresponding to transmission through an ST solar window observed from the inside. From the resulting chromaticity plot (Figure 2B), we can see that, because of the narrow absorption peaks of the devices, the color can be tuned over a wide range simply by varying the choice of organic semiconductor; this differs from organic bulk heterojunctions, in which the color depends on a more complex interaction of the optical constants of both materials and the phase behavior of the blend. This suggests that such bilayers may be well suited for optoelectronic applications with a demand for high transparency coupled with color tunability, such as color-tunable PV windows.

To demonstrate such suitability, we take the example of CuSCN/C_{60}, which has the potential for extremely low-cost manufacturing because of the low cost of CuSCN ($0.7 per gram; https://www.sigmaaldrich.com/US/en/product/aldrich/298212) and C_{60} ($45 per gram; https://mstnano.com/product/fulleren-c60/). The photopic (well-lit illumination conditions) human eye response is plotted in Figure 3A, along with the absorption spectrum of a C_{60} film and the same modeled transmission spectrum of a CuSCN/C_{60} from Figure 2A. Clearly, the CuSCN/C_{60} is well suited for a highly transparent PV window, given the high overlap of the human eye response and the transmission spectrum of the device. We calculate average visible transmittance (AVT; calculated as the average transmittance from 370–740 nm) and human perception transmittance (HPT; calculated as the average transmittance weighed by the eye response function)[23] of 65% and 77%, respectively, despite the relatively thick C_{60} layer of 65 nm. Further, in Figure 3B we plot the theoretically (assuming 100% internal quantum efficiency) achievable short circuit current (J_{sc}) as the thickness of the photoactive layer is varied from 5nm to 150 nm versus AVT and HPT and compare CuSCN/C_{60} with P3HT:PC_{60}BM, which has a similar absorption spectrum and low cost potential. Clearly, for the same theoretical J_{sc}, CuSCN/C_{60} show significantly higher transmittance values, with highly transparent PV windows (HPT > 70%) possible with a theoretical J_{sc} of greater than 7 mA cm^{-2}. This demonstrates that the CuSCN/C_{60} device has excellent wavelength selectivity outside of the visible spectrum, with only a small fraction of its photocurrent derived from visible-wavelength photons.

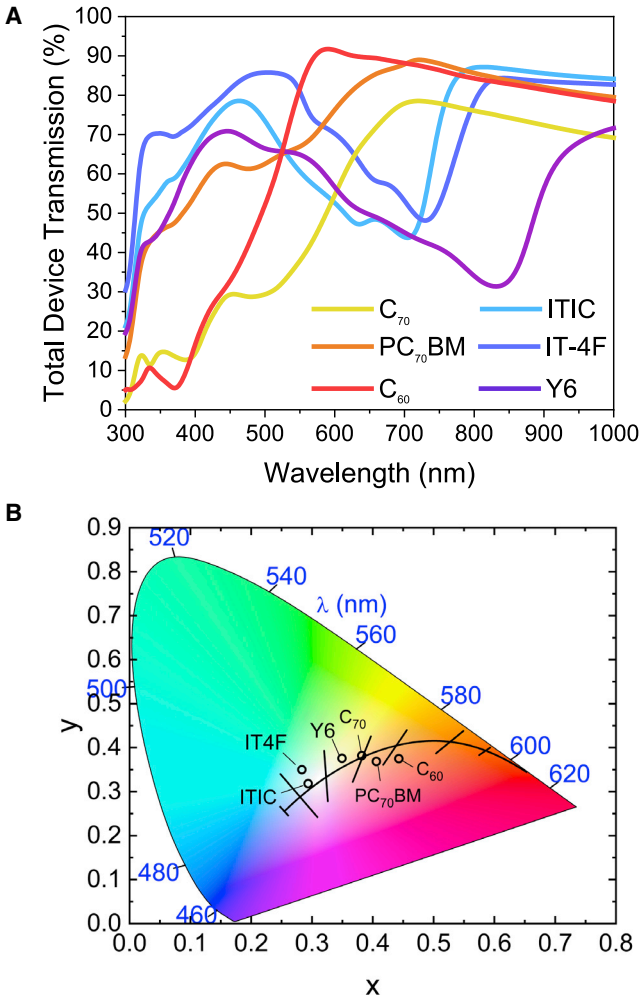

Figure 2. Color tuneability of the modeled ST PV cells

(A) Modeled transmission spectra through ST devices with the structure glass/ITO/CuSCN/organic semiconductor/BCP/ITO using ellipsometry and transfer matrix modeling. The organic semiconductor thickness in each case is optimized for maximum device PCE (~ 50 nm for C_{70}, 65 nm for C_{60}, 30 nm for ITIC and $PC_{70}BM$, and 40 nm for Y6 and IT-4F).

(B) Location of the color coordinates of all devices in a CIE 1931 chromaticity diagram, calculated from the modeled transmission of the full devices.

Another example of an application for PV windows is in the use of solar-powered integrated greenhouses, in which a ST solar cell roof covering replaces the traditional polyethylene roof. It has been shown that, to be economically and environmentally competitive with conventional greenhouses, crop yield must be maintained at a level similar to growth achieved in a greenhouse without integrated PV cells and that this can generally be achieved with high transmittance in the photosynthetically active region (PAR; 400–700 nm) compared to polyethylene.[25,26] To quantify the effect of the studied devices on the photosynthesis activity of plants, we calculate a growth factor, *G*, which is defined as

$$G = \frac{\int T(\lambda)\phi_{AM1.5}(\lambda)\alpha(\lambda)d\lambda}{\int \phi_{AM1.5}(\lambda)\alpha(\lambda)d\lambda}, \qquad \text{(Equation 1)}$$

where $T(\lambda)$ is the complete device transmission for the simulated devices, $\phi_{AM1.5}(\lambda)$ is the AM1.5 photon flux density, and $\alpha(\lambda)$ is the averaged plant action spectrum of 27

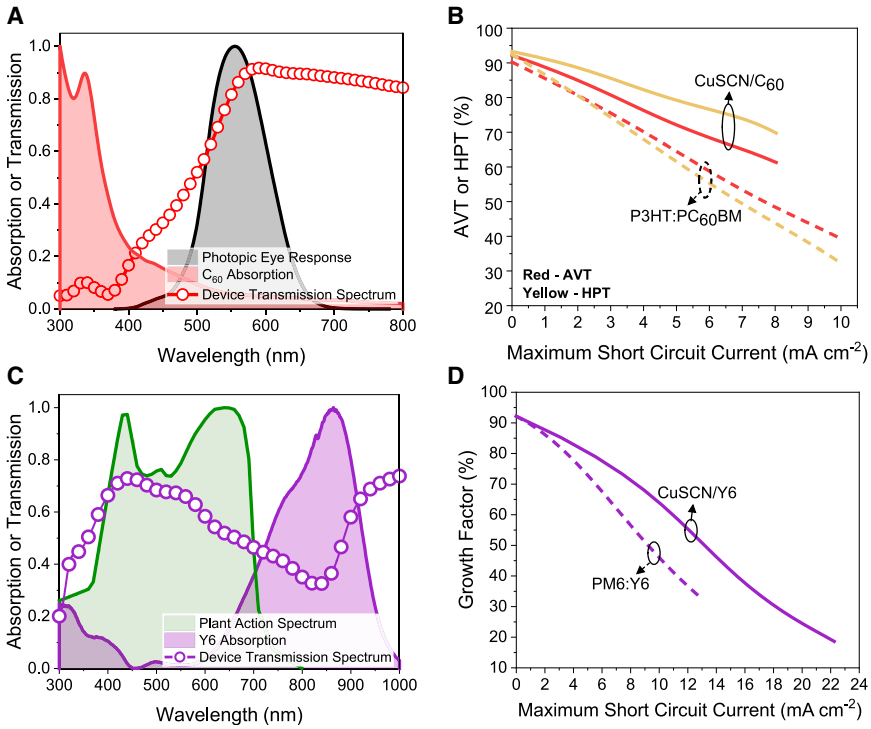

Figure 3. Modeled performance of the ST devices as PV windows

(A) Normalized photopic (under well-lit conditions) eye response spectrum (black line), normalized absorption spectrum of a C_{60} film (red line), and total device transmission spectrum of a ITO/CuSCN/C_{60} (65 nm)/BCP/ITO device (red circles).

(B) Average visible transmittance (AVT; red line) and human perception transmission (HTP; pink line) versus maximum theoretical achievable J_{sc} for a photoactive layer thickness between 5 and 150 nm.

(C) Absorption plot of the action spectrum of plants (α), the absorbance of a Y6 thin film, and the calculated transmission through a ITO/CuSCN/Y6 (30 nm) BCP/ITO ST device.

(D) Modeled growth rate as a function of maximum possible J_{sc}, assuming 100% internal qunatum efficiency for a ITO/CuSCN/Y6/BCP/ITO and a ITO/PEDOT:PSS/PM6:Y6/BCP/ITO device, using optical constants for PM6:Y6 (1:1.2 ratio) from Kerremans et al.[24] and a photoactive layer thicknesses between 5 and 100 nm.

herbaceous plants, plotted in Figure 3C.[27] *G* can be interpreted as the ratio of the photosynthetic rate in a greenhouse to the photosynthetic rate under a clear sky (assuming that the photosynthetic rate is proportional to the number of absorbed photons within the plant action spectrum). To achieve the maximum *G*, a ST PV device should absorb primarily at wavelengths longer than 700 nm, as is the case with our CuSCN/Y6 devices, as shown in Figure 3C. We thus calculate the *G* for the Y6 device to be as high as 58%, because of its favorable absorption peak in the region of 700–850 nm. This value is on par with reported values for organic bulk heterojunction (BHJ) devices when corrected for differences in power conversion efficiency (PCE)[6,28] but using a much simpler device architecture with lower potential material costs. To further demonstrate the beneficial effect of using a transparent donor such as CuSCN for applications where transparency in a particular region of the spectrum is required, we compare the achievable *G* versus the maximum achievable J_{sc} of the device with a blend of PM6:Y6, one of best-performing BHJ solar cell polymer:small molecule blends that is used widely in ST devices, at a photoactive layer thickness from 5–100 nm in Figure 3D. Evidently, the maximum achievable photocurrent at a given *G* is significantly higher for CuSCN/Y6 than for PM6:Y6 because of the

extremely high extinction coefficient of Y6 between 650 and 900 nm (Figure S1). Although we acknowledge that CuSCN/organic devices cannot compete with BHJ cells in terms of current generation above 6 mA cm^{-2} because of exciton diffusion length limits, Figures 3B and 3D demonstrate the potential of using transparent components in a heterojunction to achieve maximum achievable transparency in a given wavelength range. Growth rates as a function of organic layer thicknesses are shown for all studied materials in Figure S4.

Low-voltage-loss ST PV windows for PEC water splitting

Next we present an application that offers the possibility of combining the two main benefits of CuSCN/organic devices, color tunability and low voltage losses, by examining the application of our devices as a PV window to provide additional photovoltage to drive water oxidation in tandem with a PEC cell to generate sustainable hydrogen. In a typical water splitting device with an anode and a cathode, 1.23 V is the minimum cell voltage across the electrodes to reach electrochemical equilibrium. To induce a current to flow, several hundred millivolts above 1.23 V are typically needed to compensate for resistive losses and overpotentials that arise from thermodynamic losses related to charge carrier transport and from kinetic losses related to driving the oxygen evolution reaction and, to a lesser extent, the hydrogen evolution reaction.[29] This constraint has resulted in metal-oxide-based semiconductors such as hematite[30] or bismuth vanadate ($BiVO_4$)[31] being used predominantly in low-cost PECs for water oxidation as photoanodes because they typically possess low-lying valence band maxima with sufficient overpotential to efficiently drive water oxidation.[32] The constraints on oxidation and reduction potentials mean that oxides with wide optical gaps are needed, and even then an additional external bias is often needed for the PEC device to function efficiently. To provide the additional bias needed to drive the water splitting reactions, a PEC-PV tandem may be used.[33,34] The extra photovoltage provided by the PV can be regarded as an external bias for the PEC, with a high PV photovoltage generally being more desirable than a high photocurrent.

A simple configuration for a PEC-PV tandem is placing the PV and PEC side by side. However, this positioning does not utilize the solar spectrum as efficiently as it could. A more optically efficient configuration is one where the solar spectrum is shared between the two, maximizing the total fraction of photons utilized. The typical configuration for such a PEC-PV tandem with shared absorption spectrum is one when the PV cell is placed behind the PEC cell, at the end of the light path, as shown in Figure 4A.[35] In this configuration (denoted configuration PEC-PV), the typically narrower-band-gap PV cell absorbs the lower-energy photons transmitted by the wider-band-gap PEC cell under back illumination. However, from the perspective of optimizing light utilization, this configuration has the drawback that the light path from the photoactive component of the PEC (in this case the photoanode) to the PV includes the electrolyte, any evolved H_2 and O_2 bubbles, the membrane that separates the oxidation and reduction products (e.g., Nafion), and the cathode (e.g., a platinum or nickel mesh) when placed parallel to the photoanode to optimize potential gradient and current density distribution.[36] For an arrangement where all components are placed in tandem, parasitic light absorption through the components must be considered. A minimum 5% decrease in light transmission can be expected when using a Nafion membrane (Figure S5), and decreases between 2% and 25% in photocurrent because of H_2 bubbles,[37] up to 5% for O_2 bubbles,[38] and at least 20% when using a platinum (Pt) mesh cathode[39] have been demonstrated. Additionally, electrolyte absorption is strongly thickness and wavelength dependent and will be significant for thicknesses above 1 mm at wavelengths greater than about

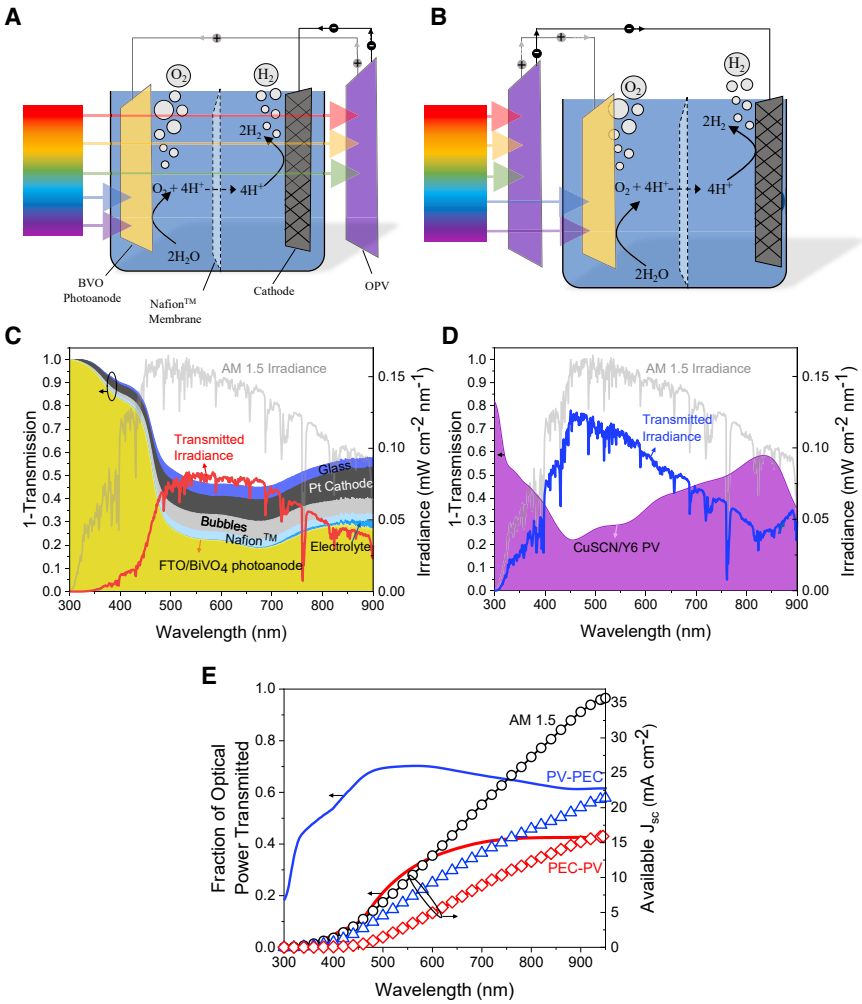

Figure 4. Comparison of the optical losses in PEC-PV and PV-PEC tandem cells

(A and B) Schematic of the photoelectrochemical (PEC)-photovoltaic (PV) tandem cell for an architecture where (A) the PV cell is placed behind the PEC and (B) where the PV is placed in front of the PEC.

(C and D) The corresponding modeled transmission losses (plotted as 1-transmission) through the front device (PEC or PV) are plotted (C) for the PEC-PV and (D) for the PV-PEC device structure, where the solar cell is CuSCN/Y6 and the photoanode is $BiVO_4$. The optical losses because of a perforated platinum cathode, bubble formation, and the membrane separating the hydrogen and oxygen evolution reactions and the rear glass optical losses are also shown. The normalized AM1.5 spectra incident on the device (gray line) and the transmitted irradiance that reaches the second light absorber in each case (red and blue lines for PEC-PV and PV-PEC, respectively) are indicated.

(E) Plot of the fraction of transmitted photon flux density (total photon flux density/transmitted photon flux density) available immediately after transmission through the first component (i.e., the PEC or PV) in both configurations as a function of wavelength. Over all wavelengths, a greater fraction of photon flux density is transmitted in the PV-PEC than in the PEC-PV configuration. Also shown is the maximum theoretical short-circuit current (J_{sc}) that could be achieved by a rear absorber with a band gap corresponding to the x axis wavelength in the Shockley-Queisser limit for each configuration.

800 nm.[40] For example, the estimated transmission losses through a PEC cell using a $BiVO_4$ photoanode coated on fluorine-doped tin oxide (FTO)-coated glass, one of the most widely used and best-performing low-cost photoanode materials,[41–45] are shown in Figure 4C, assuming 5 mm of electrolyte (modeled as water), a

moderate 10% light attenuation because of bubble formation, and a highly transmissive Pt cathode.[39] Evidently, the transmission losses through the PEC are high at all wavelengths, with around 50% transmission losses even at wavelengths longer than 500 nm where the $BiVO_4$ photoanode is not photoactive (cf. EQE, Figure S6) because of the parasitic absorption of the non-photoactive components. The transmitted irradiance after passing through the PEC (red line) compared with the incident AM1.5 irradiation (gray line) is also shown, from which the fraction of incident optical power (100 mW cm^{-2}) that reaches the PV device can be determined, as shown in Figure 4E (PEC-PV, red line). Despite the PEC utilizing only a small part of the solar spectrum (wavelengths shorter than 500 nm), the fraction of the incident photon flux density that is available to a rear PV cell with a band gap of 900 nm is only about 0.4. The maximum possible J_{sc} that can be extracted from such a PV cell therefore decreases from 34 mA cm^{-2} to 15 mA cm^{-2} after the light has passed through the PEC cell, as shown in Figure 4E, which includes 12 mA cm^{-2} of parasitic (i.e., not absorbed by the photoanode) absorption. Such optical losses (50%–60%) are in agreement with experimentally measured values in the literature.[46] A common method used to alleviate parasitic light absorption because of the cathode is to place it out of the light path.[46] However, this leads to a decrease in performance because of the unfavorable, non-homogeneous distribution of current density at the electrodes and concentration and pH gradients in the electrolyte, especially in large-scale cells, and is therefore not a favorable approach.

Although the parasitic absorption in the PEC cell is not the factor that limits the solar-to-hydrogen (STH) efficiency in current (<10% STH) tandem systems, given the much higher photocurrents exhibited by PVs compared with current-generation PECs, such parasitic absorption will increasingly matter as the performance of PECs improves toward the required 10% STH target for commercial viability.[47] One way of minimizing parasitic absorption is to use a configuration in which the PV cell is placed in front of the PEC (Figure 4B), minimizing parasitic absorption from non-photoactive components of the tandem device. In this configuration (denoted configuration PV-PEC), the typically narrower-band-gap PV cell must be as transparent as possible to the high-energy photons that can be utilized by the wider-band-gap PEC cell, which, in the case of $BiVO_4$, is wavelengths below 500 nm (see $BiVO_4$ EQE in Figure S6).[48] As we demonstrated above (Figure 2), the CuSCN-based ST devices paired with low-band-gap organic semiconductors (Y6, ITIC, and IT-4F) show good transparency to visible light with wavelengths shorter than around 550 nm and thus make excellent ST windows to provide additional voltage for water splitting for a $BiVO_4$-based PEC cell. Additionally, it is worth noting the exceptional ability of some of these heterojunctions to maintain the necessary high V_{oc} to help drive water splitting in conjunction with narrow-band absorption, something not easily achievable in a heterojunction with two organic semiconductors with similar band gaps because of the requirement to maintain appropriate energetic offsets for both electron and hole transfer.[49]

The plateau photocurrent of the $BiVO_4$ photoanode is just under 5.5 mA cm^{-2} (Figure S7), and we chose CuSCN/Y6 as the most suitable hybrid heterojunction PV device in the PEC-PV tandem because of its highest J_{sc} (6.4 mA cm^{-2}) and its complementary spectral response to $BiVO_4$. The transmission loss spectrum of an optimized CuSCN/Y6 (with a Y6 thickness of 30 nm) device is shown in Figure 4D (purple), noting again that, in this configuration, there are no non-photoactive components in the light path between the (front) PV and the (back) PEC device. Cleary, the PV is highly transmissive between 350 and 500 nm, with a transmission loss minimum of around 25% at 450 nm, which translates to only a small loss in transmitted irradiance

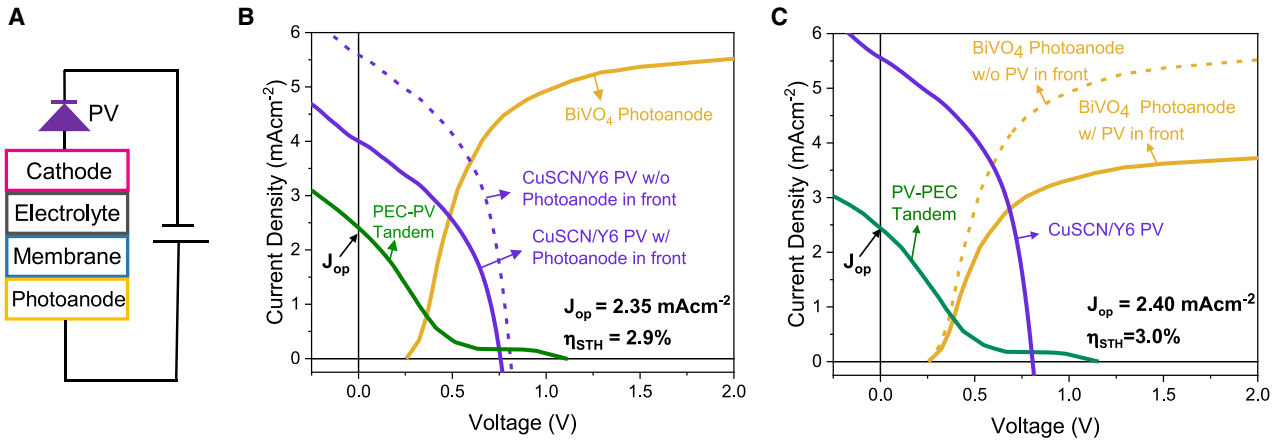

Figure 5. Modeled performance of PV-PV and PV-PV tandem cells using a joint electric-optical model

(A) Illustration of the electrical model used to model PV-PEC tandem cells.

(B and C) JV plot of photoactive components in the system for the same $BiVO_4$-based PEC connected in tandem with the CuSCN/Y6 PV cell in the PEC-PV (B) and PV-PEC (C) configuration. The operating current (J_{op}) for unassisted water splitting is the current at zero overall bias of the whole device (green line) and is given by the intersection of the PEC (solid yellow line) and PV (purple) curves minus other resistive losses (gray, electrolyte; blue, membrane; pink, Pt cathode). The resistive losses included in the calculation are shown graphically in Figure S8. Note that the thickness of Y6 is 30 nm in the PEC-PV and PV-PEC configurations, respectively, chosen to maximize the STH efficiency of the whole device.

(blue line) that reaches the rear PEC. The fraction of photon flux density compared with the incident irradiation that can be used by the $BiVO_4$ photoanode (absorption cutoff at 500 nm) is therefore almost 0.7, as shown in Figure 4E (blue line), corresponding to a drop in the maximum theoretically available photocurrent of the PEC from 6.5 to 4.5 mA cm^{-2} (blue triangles). Optical losses through the PV remain low until around 600 nm, when a photocurrent of around 9.5 mA cm^{-2} of photocurrent would be theoretically reachable by a PEC with this band gap. It is evident, therefore, that optical losses in the PV-PEC configuration compare favorably with the PEC-PV configuration because of the minimizing of parasitic absorption by non-photoactive components.

To compare the performance of the two configurations, we proceed to model the water splitting performance of such a PEC-PV cell using the above optical model in conjunction with the electrical model shown in Figure 5A, in which all electrical (photoanode, cathode, membrane, electrolyte, and PV) components are connected in series to calculate the current-voltage (JV) curve of the total PEC-PV tandem device. For the photoactive component (photoanode or PV) at the front of the tandem stack, we use experimentally measured JV curves for the $BiVO_4$ photoanode[48,50,51] and CuSCN/Y6 PV,[20] corresponding to the devices used in Figure 4. For the photoactive component at the rear of the tandem stack, we calculate the JV behavior using the modeled optical losses from Figure 4 and assuming the superposition principle and a linear dependence of the photocurrent on light intensity for the PV and photoanode, respectively. The JV behavior of the non-photoactive components (cathode, membrane, and electrolyte) are taken from literature.[47,48]

The operating point of the full PEC-PV tandem device is then given by the intersection of the photoanode and PV JV curves under illumination minus the resistive losses induced by the cathode, electrolyte, and membrane. The value at which the total PEC-PV tandem JV curve crosses the y axis thus defines the maximum operating current, J_{op}, that can be used to drive the water splitting reaction at zero external bias. To minimize coupling losses, this operating point should be close to

the maximum power points of the PEC and PV devices, meaning that the currents of both devices should be matched while extracting the maximum possible voltage.

The JV curves of the PEC-PV and PV-PEC device configurations are given in Figures 5B and 5C, respectively. The $BiVO_4$ photoanode (yellow) and CuSCN/Y6 PV (purple) JV curves as well as the modeled PEC-PV (green) JV curves (including resistive losses) are shown, with the current voltage curves of the individual resistive components shown in Figure S8. A comparison of the two configurations reveals that the PV-PEC configuration can operate at a slightly higher operating current (2.40 mA cm^{-2}) than the PEC-PV configuration (2.35 mA cm^{-2}), yielding a higher STH efficiency of 3.0% (assuming 100% faradic efficiency of H_2 evolution) compared with 2.9%. The PV-PEC configuration slightly outperforms PEC-PV because of the large optical losses through the PEC cell in the PEC-PV configuration that lead to a mismatch in the photocurrent outputs of the PV and PEC cell. This results in the PV-PEC device operating closer to the maximum operating points of the PEC and PV than in the PEC-PV configuration. Further improvements in the efficiency of the tandem device could be achieved using a photoanode with a higher photocurrent or by further increasing the V_{oc} of the PV device. Relatively high STH efficiencies can be achieved in both configurations even when using a simple bilayer single-junction solar cell, as opposed to multijunction PV tandem cells commonly employed in PEC-PV tandems,[48] because of the high V_{oc} of the CuSCN/Y6 cell coupled with its excellent complementary absorption window to the PEC device.

This result demonstrates that a PV-PEC tandem configuration can be a competitive alternative to a PEC-PV configuration when using highly ST PV devices. This is especially intriguing in the context of achieving around 10%–20% STH efficiency, necessary for PEC water splitting to be competitive with electrolysis.[24,52] For current PEC-PV tandem devices, the high optical losses in the PEC-PV configuration are not necessarily a problem because the low photocurrent possible by current state-of-the-art photoanodes ($\sim$ 5 $mAcm^{-2}$) is easily matched by commercial silicon PV cells even after optical losses. However, for achieving, for example, a 15% STH efficiency, operating current densities beyond 13 mA cm^{-2} are required. This makes reducing parasitic optical losses in such a system paramount for the PEC and PV to be able to operate at such current densities. The PV-PEC configuration explored in this contribution may offer such a solution.

DISCUSSION

Here we demonstrated that CuSCN/organic heterojunctions can be used to build optoelectronic devices with absorption spectra tunable solely by the choice of the organic semiconductor. We first demonstrated that easily color-tunable PV cells can be designed for use in applications such as greenhouses or ST windows, with higher theoretical transmittance (AVT, *G*, and HPT) for equivalent J_{sc} than with conventional BHJ organic solar cells, leaving a greater fraction of the solar spectrum available for other functions, such as plant growth or building lighting.

Further, the benefit of pairing a transparent donor with a light-absorbing acceptor is demonstrated by modeling the devices as ST windows for PEC-PV tandem cells for water splitting, made possible by the unique combination of high V_{oc} and transparency at short wavelengths of some of the CuSCN/organic bilayers. By placing the ST PV cells in front of the PEC device, most parasitic light absorption losses are avoided and higher STH efficiencies are achieved compared with the conventional architecture, where the PV is placed behind the PEC device.

We suggest that, although the demonstrated efficiencies using these hybrid heterojunctions are not sufficient to compete with all-organic or all-inorganic heterojunctions, the current study demonstrates the potential benefit of using heterojunction devices with only a single photoactive component, allowing precise and simple color tunability without sacrificing V_{oc}. Additionally, the current study illustrates the importance of optical light management in PEC-PV tandems, especially in the context of achieving STH efficiencies necessary for making such devices competitive with other hydrogen-generating technologies.

EXPERIMENTAL PROCEDURES

Resource availability

Lead contact

Further information and requests for resources and reagents should be directed to and will be fulfilled by the lead contact, Flurin Eisner (f.eisner15@imperial.ac.uk).

Materials availability

This study did not generate new unique reagents.

Data and code availability

The published article and associated supplemental information includes all of the necessary data required for evaluating the main findings of this study. Any additional data related to this study are available from the lead contact upon request.

Ultraviolet-visible near-infrared absorption measurements

For absorption measurements, films were deposited on quartz, and the transmission and diffuse reflection of the films were measured using a Shimadzu UV-2600 spectrophotometer equipped with an ISR-2600Plus integrating sphere. The absorption of the sample was calculated from the transmission and reflection measurements by comparison with the measurements of a reference clean quartz substrate.

Ellipsometry measurements

Variable-angle spectroscopic ellipsometry (VASE) measurements were performed using a SOPRALAB GES5E rotating polarizer ellipsometer with a Xe lamp as a light source and a charge-coupled device (CCD) detector to record optical spectra from 1.2–5.6 eV. Three incidence angles were typically recorded for each sample, varying between 55° and 75°.

Optical and electrical modeling of PV cells

Light propagation through the device stack was modeled using transfer matrix calculations using the optical data measured from ellipsometry. The JV curves of PV devices at different thicknesses and using ITO cathodes were modeled by applying the superposition principle to the experimentally measured optimum JV curves for opaque devices (Figure 1), using the measured internal quantum efficiency and calculated absorptions to calculate the J_{sc}. We assume the internal quantum efficiency to be independent of thickness and cap the thickness at the optimum thickness for power conversion efficiency in opaque cells to not overestimate the performance of the devices.

Optical and electrical modeling of PEC cells

The high roughness of nanotextured $BiVO_4$ photoanodes makes measuring optical constants unreliable. Because of additional difficulties in measuring optical constants for bubble formation and perforated platinum cathodes as well as the

unsuitability of using transfer matrix approaches for modeling optical propagations through thick (>1 cm) liquid environments, we instead adopted a simple model using the fractional optical losses of each subsequent material in the device stack using transmission and reflection data of the materials. For FTO/$BiVO_4$, Nafion membrane, and glass, we experimentally measured the transmission spectra, and we used experimental data from the literature for the platinum electrode[39] and aqueous electrolyte.[40] For bubble formation, we assumed a wavelength-dependent optical loss of 10%.[38] The calculated loss values are in agreement with experimental results from the literature.[46]

Optical and electrical modeling of PEC-PV tandem cells

For PEC-PV tandem cells in which the PV device is situated behind the PEC, the fraction of the AM1.5 illumination reaching the PV was reduced by the transmission spectra of the PEC, electrolyte, and Nafion membrane. The JV curves of the subcells were recalculated using the reduced illumination intensity through the superposition principle, yielding the reconstructed tandem PV JV in the same manner as above. For a device configuration in which the PV device is situated in front of the PEC cell, the fraction of illumination reaching the PEC cell was reduced by the modeled transmission through the PV cell, and the JV of the PEC cell was recalculated, assuming a linear dependence of the photocurrent on light intensity.

The JV of the tandem PV-PEC device was calculated using the equivalent circuit diagram shown in Figure 5A and assuming no other electrical losses. The electrolyte resistance was taken from Hernández-Pagán et al.[51] (10 ohm/cm^2), and the Nafion membrane resistance was taken from the manufacturer's data sheet (0.127 ohm/cm^2; https://www.fuelcellsetc.com/store/N115). The JV of the Pt mesh was taken from Urbain et al.[50]

SUPPLEMENTAL INFORMATION

Supplemental information can be found online at https://doi.org/10.1016/j.xcrp.2021.100676.

ACKNOWLEDGMENTS

F.E. thanks the Engineering and Physical Sciences Research Council (EPSRC) for support via a postdoctoral prize fellowship. J.N. is grateful for funding from the EPSRC (grants EP/ P005543/1 and EP/M025020/1) and the European Research Council (ERC) under the European Union Horizon 2020 Research and Innovation Program (grant agreement 742708). M.C.Q. and V.B. thank the ERC through support via grant agreement 648901. B.T. thanks the Imperial College President's Ph.D. scholarship scheme. A.K. thanks the Imperial College for a junior research fellowship, the EPSRC for a Capital Award Emphasising Support for Early Career Researchers, and the Royal Society for an equipment grant (RSG\R1\180434).

AUTHOR CONTRIBUTIONS

F.E. and J.N. conceptualized and designed the idea and model and directed the research. F.E. wrote the draft manuscript. F.E., B.T., and W.O. carried out the modeling of semi-transparent PV devices and PEC-PV tandems. V.B. and M.C.-Q. carried out the ellipsometry measurements and calculated the refractive indices. J.Y. and M.A. provided guidance with the modeling of semi-transparent PV devices. A.K. and A.H. helped with the underlying theory and modeling of PV-PEC tandem devices. All authors contributed toward the discussion of the results and revision of the manuscript.

DECLARING OF INTERESTS

The authors declare no competing interests.

Received: September 21, 2021
Revised: November 2, 2021
Accepted: November 15, 2021
Published: December 6, 2021

REFERENCES

1. Riede, M., Spoltore, D., and Leo, K. (2021). Organic Solar Cells—The Path to Commercial Success. Adv. Energy Mater. *11*, 2002653.

2. Dai, S., and Zhan, X. (2018). Nonfullerene Acceptors for Semitransparent Organic Solar Cells. Adv. Energy Mater. *8*, 1800002.

3. Pulli, E., Rozzi, E., and Bella, F. (2020). Transparent photovoltaic technologies: Current trends towards upscaling. Energy Convers. Manage. *219*, 112982.

4. Ravishankar, E., Booth, R.E., Saravitz, C., Sederoff, H., Ade, H.W., and O'Connor, B.T. (2020). Achieving Net Zero Energy Greenhouses by Integrating Semitransparent Organic Solar Cells. Joule *4*, 490–506.

5. Ravishankar, E., Charles, M., Xiong, Y., Henry, R., Swift, J., Rech, J., Calero, J., Cho, S., Booth, R.E., Kim, T., et al. (2021). Balancing crop production and energy harvesting in organic solar-powered greenhouses. Cell Reports Physical Science *2*, 100381.

6. Emmott, C.J.M., Röhr, J.A., Campoy-Quiles, M., Kirchartz, T., Urbina, A., Ekins-Daukes, N.J., and Nelson, J. (2015). Organic photovoltaic greenhouses: a unique application for semi-transparent PV? Energy Environ. Sci. *8*, 1317–1328.

7. Li, X., Xia, R., Yan, K., Yip, H.-L., Chen, H., and Li, C.-Z. (2020). Multifunctional semitransparent organic solar cells with excellent infrared photon rejection. Chin. Chem. Lett. *31*, 1608–1611.

8. Li, Y., Guo, X., Peng, Z., Qu, B., Yan, H., Ade, H., Zhang, M., and Forrest, S.R. (2020). Color-neutral, semitransparent organic photovoltaics for power window applications. Proc. Natl. Acad. Sci. USA *117*, 21147–21154.

9. Cui, Y., Yang, C., Yao, H., Zhu, J., Wang, Y., Jia, G., Gao, F., and Hou, J. (2017). Efficient Semitransparent Organic Solar Cells with Tunable Color enabled by an Ultralow-Bandgap Nonfullerene Acceptor. Adv. Mater. *29*, 1703080.

10. Rodríguez-Martínez, X., Pascual-San-José, E., Fei, Z., Heeney, M., Guimerà, R., and Campoy-Quiles, M. (2021). Predicting the photocurrent–composition dependence in organic solar cells. Energy Environ. Sci. *14*, 986–994.

11. Rodríguez-Martínez, X., Pascual-San-José, E., and Campoy-Quiles, M. (2021). Accelerating organic solar cell material's discovery: high-throughput screening and *big data*. Energy Environ. Sci. *14*, 3301–3322.

12. Huang, X., Oh, J., Cheng, Y., Huang, B., Ding, S., He, Q., Wu, F., Yang, C., Chen, L., and Chen, Y. (2021). Narrow band-gap materials with overlapping absorption simultaneously increase the open circuit voltage and average visible transmittance of semitransparent organic solar cells. J. Mater. Chem. A Mater. Energy Sustain. *9*, 5711–5719.

13. Jiang, T., Zhang, G., Xia, R., Huang, J., Li, X., Wang, M., Yip, H.L., and Cao, Y. (2021). Semitransparent organic solar cells based on all-low-bandgap donor and acceptor materials and their performance potential. Mater. Today Energy *21*, 100807.

14. Panda, A., Renshaw, C.K., Oskooi, A., Lee, K., and Forrest, S.R. (2014). Excited state and charge dynamics of hybrid organic/inorganic heterojunctions. II. Experiment. Phys. Rev. B *90*.

15. Renshaw, C.K., and Forrest, S.R. (2014). Excited state and charge dynamics of hybrid organic/inorganic heterojunctions. I. Theory. Phys. Rev. B *90*.

16. Firdaus, Y., Seitkhan, A., Eisner, F., Sit, W.-Y., Kan, Z., Wehbe, N., Balawi, A.H., Yengel, E., Karuthedath, S., Laquai, F., and Anthopoulos, T.D. (2018). Charge Photogeneration and Recombination in Mesostructured CuSCN-Nanowire/$PC_{70}BM$ Solar Cells. Sol. RRL *2*, 1800095.

17. Sit, W.Y., Eisner, F.D., Lin, Y.H., Firdaus, Y., Seitkhan, A., Balawi, A.H., Laquai, F., Burgess, C.H., McLachlan, M.A., Volonakis, G., et al. (2018). High-Efficiency Fullerene Solar Cells Enabled by a Spontaneously Formed Mesostructured CuSCN-Nanowire Heterointerface. Adv. Sci. (Weinh.) *5*, 1700980.

18. Karuthedath, S., Gorenflot, J., Firdaus, Y., Sit, W.-Y., Eisner, F., Seitkhan, A., Ravva, M.K., Anthopoulos, T.D., and Laquai, F. (2019). Charge and Triplet Exciton Generation in Neat PC70BM Films and Hybrid CuSCN:PC70BM Solar Cells. Adv. Energy Mater. *9*, 1802476.

19. Firdaus, Y., Le Corre, V.M., Karuthedath, S., Liu, W., Markina, A., Huang, W., Chattopadhyay, S., Nahid, M.M., Nugraha, M.I., Lin, Y., et al. (2020). Long-range exciton diffusion in molecular non-fullerene acceptors. Nat. Commun. *11*, 5220.

20. Eisner, F., Foot, G., Yan, J., Azzouzi, M., Georgiadou, D.G., Sit, W.Y., Firdaus, Y., Zhang, G., Lin, Y.-H., Yip, H.-L., et al. (2021). Emissive Charge-Transfer States at Hybrid Inorganic/Organic Heterojunctions Enable Low Non-Radiative Recombination and High-Performance Photodetectors. Adv. Mater. 2104654.

21. Pattanasattayavong, P., Promarak, V., and Anthopoulos, T.D. (2017). Electronic Properties of Copper(I) Thiocyanate (CuSCN). Adv. Electron. Mater. *3*, 1600378.

22. Eisner, F. (2019). Spectroscopic studies of the charge-transfer state and device performance of hybrid and organic solar cells (Imperial College London), PhD thesis.

23. Pascual-San-José, E., Sadoughi, G., Lucera, L., Stella, M., Martínez-Ferrero, E., Morse, G.E., Campoy-Quiles, M., and Burgués-Ceballos, I. (2020). Towards photovoltaic windows: scalable fabrication of semitransparent modules based on non-fullerene acceptors via laser-patterning. J. Mater. Chem. A Mater. Energy Sustain. *8*, 9882–9895.

24. Kerremans, R., Kaiser, C., Li, W., Zarrabi, N., Meredith, P., and Armin, A. (2020). The Optical Constants of Solution-Processed Semiconductors—New Challenges with Perovskites and Non-Fullerene Acceptors. Adv. Opt. Mater. *8*, 2000319.

25. Hollingsworth, J.A., Ravishankar, E., O'Connor, B., Johnson, J.X., and DeCarolis, J.F. (2020). Environmental and economic impacts of solar-powered integrated greenhouses. J. Ind. Ecol. *24*, 234–247.

26. Baxevanou, C., Fidaros, D., Katsoulas, N., Mekeridis, E., Varlamis, C., Zachariadis, A., and Logothetidis, S. (2020). Simulation of Radiation and Crop Activity in a Greenhouse Covered with Semitransparent Organic Photovoltaics. Appl. Sci. (Basel) *10*, 2550.

27. Inada, K. (1976). Action spectra for photosynthesis in higher plants. Plant Cell Physiol. *17*, 355–365.

28. Shi, H., Xia, R., Zhang, G., Yip, H.-L., and Cao, Y. (2019). Spectral Engineering of Semitransparent Polymer Solar Cells for Greenhouse Applications. Adv. Energy Mater. *9*, 1803438.

29. Jiang, C., Moniz, S.J.A., Wang, A., Zhang, T., and Tang, J. (2017). Photoelectrochemical devices for solar water splitting - materials and challenges. Chem. Soc. Rev. *46*, 4645–4660.

30. Le Formal, F., Tétreault, N., Cornuz, M., Moehl, T., Grätzel, M., and Sivula, K. (2011). Passivating surface states on water splitting hematite photoanodes with alumina overlayers. Chem. Sci. (Camb.) *2*, 737–743.

31. Seabold, J.A., and Choi, K.-S. (2012). Efficient and stable photo-oxidation of water by a bismuth vanadate photoanode coupled with an iron oxyhydroxide oxygen evolution catalyst. J. Am. Chem. Soc. *134*, 2186–2192.

32. Sivula, K., and van de Krol, R. (2016). Semiconducting materials for photoelectrochemical energy conversion. Nat. Rev. Mater. *1*, 15010.

33. Zhang, K., Ma, M., Li, P., Wang, D.H., and Park, J.H. (2016). Water Splitting Progress in Tandem Devices: Moving Photolysis beyond Electrolysis. Adv. Energy Mater. *6*, 1600602.

34. Prévot, M.S., and Sivula, K. (2013). Photoelectrochemical Tandem Cells for Solar Water Splitting. J. Phys. Chem. C *117*, 17879–17893.

35. Moss, B., Babacan, O., Kafizas, A., and Hankin, A. (2021). A Review of Inorganic Photoelectrode Developments and Reactor Scale-Up Challenges for Solar Hydrogen Production. Adv. Energy Mater. *11*, 2003286.

36. Hankin, A., Bedoya-Lora, F.E., Ong, C.K., Alexander, J.C., Petter, F., and Kelsall, G.H. (2017). From millimetres to metres: the critical role of current density distributions in photo-electrochemical reactor design. Energy Environ. Sci. *10*, 346–360.

37. Dorfi, A.E., West, A.C., and Esposito, D.V. (2017). Quantifying Losses in Photoelectrode Performance Due to Single Hydrogen Bubbles. J. Phys. Chem. C *121*, 26587–26597.

38. Holmes-Gentle, I., Bedoya-Lora, F., Alhersh, F., and Hellgardt, K. (2019). Optical Losses at Gas Evolving Photoelectrodes: Implications for Photoelectrochemical Water Splitting. J. Phys. Chem. C *123*, 17–28.

39. Holmes-Gentle, I., Hoffmann, F., Mesa, C.A., and Hellgardt, K. (2017). Membrane-less photoelectrochemical cells: product separation by hydrodynamic control. Sustain. Energy Fuels *1*, 1184–1198.

40. Döscher, H., Geisz, J.F., Deutsch, T.G., and Turner, J.A. (2014). Sunlight absorption in water – efficiency and design implications for photoelectrochemical devices. Energy Environ. Sci. *7*, 2951–2956.

41. Chatchai, P., Murakami, Y., Kishioka, S.-y., Nosaka, A.Y., and Nosaka, Y. (2009). Efficient photocatalytic activity of water oxidation over WO3/BiVO4 composite under visible light irradiation. Electrochim. Acta *54*, 1147–1152.

42. Su, J., Guo, L., Bao, N., and Grimes, C.A. (2011). Nanostructured $WO_3/BiVO_4$ heterojunction films for efficient photoelectrochemical water splitting. Nano Lett. *11*, 1928–1933.

43. Pihosh, Y., Turkevych, I., Mawatari, K., Uemura, J., Kazoe, Y., Kosar, S., Makita, K., Sugaya, T., Matsui, T., Fujita, D., et al. (2015). Photocatalytic generation of hydrogen by core-shell $WO_3/BiVO_4$ nanorods with ultimate water splitting efficiency. Sci. Rep. *5*, 11141.

44. Liu, Y., Wygant, B.R., Kawashima, K., Mabayoje, O., Hong, T.E., Lee, S.-G., Lin, J., Kim, J.-H., Yubuta, K., Li, W., et al. (2019). Facet effect on the photoelectrochemical performance of a WO3/BiVO4 heterojunction photoanode. Appl. Catal. B *245*, 227–239.

45. Selim, S., Francàs, L., García-Tecedor, M., Corby, S., Blackman, C., Gimenez, S., Durrant, J.R., and Kafizas, A. (2019). $WO_3/BiVO_4$: impact of charge separation at the timescale of water oxidation. Chem. Sci. (Camb.) *10*, 2643–2652.

46. Ahmet, I.Y., Ma, Y., Jang, J.-W., Henschel, T., Stannowski, B., Lopes, T., Vilanova, A., Mendes, A., Abdi, F.F., and van de Krol, R. (2019). Demonstration of a 50 cm2 BiVO4 tandem photoelectrochemical-photovoltaic water splitting device. Sustain. Energy Fuels *3*, 2366–2379.

47. Durrant, J.R., and Hammarström, L. (2019). Mission Innovation Challenge "Converting Sunlight". http://mission-innovation.net/wp-content/uploads/2019/11/IC5-Cambridge-2019-Draft-1.pdf.

48. Kim, J.H., Hwang, S.M., Hwang, I., Han, J., Kim, J.H., Jo, Y.H., Seo, K., Kim, Y., and Lee, J.S. (2019). Seawater-Mediated Solar-to-Sodium Conversion by Bismuth Vanadate Photoanode-Photovoltaic Tandem Cell: Solar Rechargeable Seawater Battery. iScience *19*, 232–243.

49. Azzouzi, M., Kirchartz, T., and Nelson, J. (2019). Factors Controlling Open-Circuit Voltage Losses in Organic Solar Cells. Trends Chem. *1*, 49–62.

50. Urbain, F., Smirnov, V., Becker, J.-P., Rau, U., Ziegler, J., Kaiser, B., Jaegermann, W., and Finger, F. (2015). Application and modeling of an integrated amorphous silicon tandem based device for solar water splitting. Sol. Energy Mater. Sol. Cells *140*, 275–280.

51. Hernández-Pagán, E.A., Vargas-Barbosa, N.M., Wang, T., Zhao, Y., Smotkin, E.S., and Mallouk, T.E. (2012). Resistance and polarization losses in aqueous buffer–membrane electrolytes for water-splitting photoelectrochemical cells. Energy Environ. Sci. *5*, 7582–7589.

52. Shaner, M.R., Atwater, H.A., Lewis, N.S., and McFarland, E.W. (2016). A comparative technoeconomic analysis of renewable hydrogen production using solar energy. Energy Environ. Sci. *9*, 2354–2371.